



-50%
reduction in unplanned
transfers over a 10-year
period⁵

-60%
reduction in rescue
events over a 10-year
period⁵

Improving Outcomes on the General Ward with **Patient SafetyNet™**

Remote Monitoring
and Clinician Notification System

[LEARN MORE](#)





Versatile lysine dendrigrafts and polyethylene glycol hydrogels with inherent biological properties: *in vitro* cell behavior modulation and *in vivo* biocompatibility.

Mariana Carranca^{1,2}, Louise Griveau^{1,2}, Noëlle Remoué¹, Chloé Lorion¹, Pierre Weiss³, Valérie Orea¹, Dominique Sigaudou-Roussel¹, Clément Faye^{4#}, Daniel Ferri-Angulo², Romain Debret¹, Jérôme Sohier^{1,2}

¹CNRS Université Lyon 1, UMR 5305, Laboratory of Tissue Biology and Therapeutic Engineering, IBCP, 7 Passage du Vercors, 69367 Lyon Cedex 07, France

²CNRS INSA, UMR 5510, Laboratory for Materials Engineering and Science, Bat. B. Pascal, 7 Avenue Jean Capelle 69621 Villeurbanne Cedex, France

³INSERM, UMR_S 791, Laboratory of Osteo-Articular and Dental Engineering, 1 Place Alexis Ricordeau, 44042 Nantes, France

⁴COLCOM, Bat CAP ALPHA, 9 avenue de l'Europe 34830 Clapiers, France

[#]Current address : GLPBiocontrol, Bat CAP ALPHA, 9 avenue de l'Europe 34830, Clapiers, France

Author information:

Corresponding author: Jérôme Sohier

E-mail: jerome.sohier@insa-lyon.fr

Abstract:

Poly(ethylene glycol) (PEG) hydrogels have been extensively used as scaffolds for tissue engineering applications, owing to their biocompatibility, chemical versatility and tunable mechanical properties. However, their bio-inert properties require them to be associated with additional functional moieties to interact with cells. To circumvent this need, we propose here to reticulate PEG molecules with poly(L-lysine) dendrigrafts (DGL) to provide intrinsic cell functionalities to PEG-based hydrogels. The physico-chemical characteristics of the resulting hydrogels were studied in regard of the concentration of each component. With increasing amounts of DGL, the cross-linking time and swelling ratio could be decreased, conversely to mechanical properties, which could be tailored from 7.7 ± 0.7 to 90 ± 28.8 kPa. Furthermore, fibroblasts adhesion, viability and morphology on hydrogels were then assessed. While cell adhesion significantly increased with the concentration of DGL, cell viability was dependant of the ratio of DGL and PEG. Cell morphology and proliferation, however appeared mainly related to the overall hydrogel rigidity. To allow cell infiltration and cell growth in 3D, the hydrogels were rendered porous. The biocompatibility of resulting hydrogels of different compositions and porosities was evaluated by 3-week subcutaneous implantations in mice. Hydrogels allowed an extensive cellular infiltration with a mild foreign body reaction, histological evidence of hydrogel degradation and neovascularization.

This article has been accepted for publication and undergone full peer review but has not been through the copyediting, typesetting, pagination and proofreading process which may lead to differences between this version and the Version of Record. Please cite this article as doi: 10.1002/jbm.a.37083

Keywords: PEG based Hydrogels; Mechanical Properties; Poly(L-lysine) Dendrimers; Cell interaction; Biocompatibility

Accepted Article

1. Introduction

The interest in hydrogels has grown rapidly in the past decade due to their vast potential in tissue engineering, tissue regeneration and drug delivery.⁽¹⁾ These hydrophilic polymer networks are of interest through their biocompatibility, viscoelasticity, permeability to oxygen and nutrients, and high water content.^{(2)–(4)} While natural hydrogels (e.g., collagen, gelatin, fibrin) confer their inherent extracellular matrix (ECM) structure and qualities, they often show weak mechanical properties, batch-to-batch variability⁽⁵⁾ and risk of pathogen transfer.⁽⁶⁾ Conversely, synthetic hydrogels have an exact composition and multi-tunable properties, but may lack bioactivity to promote cellular activities.^{(3),(7),(8)} Among these, PEG hydrogels have been extensively used for controlled drug delivery, as cell vehicles or tissue engineering scaffolds over the past decades, owing to their excellent biocompatibility, chemical versatility and tunable mechanical properties⁽⁹⁾. However, in the context of tissue engineering, a corollary setback of their bio-inert nature is that they require to be associated, functionalized or coated with supplementary proteins of the native ECM or functional moieties, such as collagen⁽¹⁰⁾, laminin⁽¹¹⁾, or arginine-glycine-aspartic (RGD) peptides^{(12),(13)} to support the survival or function of adherent cells.^{(7),(14)–(16)} This necessity induces a complexification of the PEG-based hydrogel approaches for tissue engineering, which would benefit from inherent and native interactions with cells, without added factors.

PEG hydrogels can be obtained via covalent cross-links between PEG molecules through different paths, in which the PEG molecules are either functionalized with reactive end groups (e.g. methacrylate, acrylate)^{(7),(17)} and activated by initiators or associated with multifunctional monomers to avoid the use of initiators. In the latter approach, dendrimers have shown potential as cross-linking monomers, thanks to their versatile chemical composition, highly organized 3D arborescent structure and ease of surface functionalization.^{(18)–(21)} Poly(amidoamine) (PAMAM) dendrimers, for instance, have been successfully associated with PEG to form hydrogels for drug delivery applications that do not require interactions with cells^{(22)–(24)}, since they tend to exhibit unwanted features such as cytotoxicity and non-degradability⁽²⁵⁾.

Conversely, other dendritic structures with amine end groups, such as poly(L-lysine) dendrigrafts (DGL), have recently developed interest in several applications, due to their large surface area, versatility to be functionalized, water solubility, stability under sterilization conditions, partial degradability under the action of endogenous peptidases, non-immunogenicity and low cytotoxicity.^{(26),(27)} Moreover, their polycationic nature at physiological pH allows cellular adhesion,^{(27),(28)} which could be of high interest to provide cell interaction to inert materials. Indeed, DGL used as coatings on surfaces have been shown to increase cellular adhesion and proliferation of human skin fibroblasts by inducing the expression of integrin $\alpha 5$, a receptor

implied in cell adhesion to fibronectin (through RGD). In this manner the DGL could provide a bioactivity to the otherwise bio-inert material, while remaining synthetic and controllable.⁽²⁹⁾ DGL synthesis is based on the grafting of subsequent lysine molecules onto a polymeric substructure, linear poly-L-lysine (PLL), using protect-deprotect steps. In this manner, increasing generations of DGL (G1-G5) can be obtained with a simple, scalable procedure, water-soluble reaction (pH 6.5) with low batch-to-batch variability with a typical yield of 50-60% on a multigram scale.⁽³⁰⁾ While DGL-G3 and G4 showed a better cellular adhesion compared to PLL, in this study we focused on G3 since it presented the best compromise between biological activity and fabrication cost, as well as limits the formation of aggregates observed in the G4 synthesis.⁽²⁹⁾

Interestingly, DGL-G3 has never been evaluated as cross-linking monomers to form PEG hydrogels, while such hydrogels could benefit from their inherent bioactivity, without the need for further association with additional functional moieties. To create such PEG hydrogels with intrinsic interactions with cells, we hypothesized that the amine groups present in high density at the DGLs surface could be used as binding sites to form network chains through of amide bonds between activated PEG-NHS ester and DGL-G3.

We here assess these possibilities through the development of a novel hydrogel composed of DGL-G3 and PEG, with extensive and straightforward tuneable mechanical properties, to serve as matrix

Accepted Article

or cell support for soft tissue engineering applications.⁽¹⁵⁾ The characteristics of these hydrogels as cross-linking time, swelling and mechanical properties were determined. Cell interactions with the hydrogels (adhesion, viability, proliferation and morphology of dermal fibroblasts on dense hydrogels) were determined, in relation to hydrogel composition. Additionally, to allow cell colonisation and infiltration, hydrogels were rendered porous by particulate/leaching technique and their biocompatibility was determined by *in vivo* subcutaneous implantations in mice.

2. Materials and Methods

2.1. Preparation of dense DGL/PEG hydrogels

Dense hydrogels of different ratios of DGL/PEG were prepared by adding the desired concentration of PEG-bis(N-succinimidyl succinate) (PEG-NHS, 2000 g/mol, Sigma-Aldrich) in anhydrous dimethylformamide (DMF, Sigma Aldrich), to a solution of DGL (third generation, 22000 g/mol, COLCOM)⁽³¹⁾ in phosphate-buffered saline (PBS), at 4°C. For mechanical and swelling testing, 800µl hydrogels were prepared in 2ml conic tubes (Maxymum Recovery, Axygen). After cross-linking, the conical bottom of the tubes was cut off, and the tubes were immersed in ethanol for 5 min to subsequently retrieve the hydrogels. The resulting cylindrical hydrogels were then sectioned (2 mm thickness) using a vibratome (7550 Integraslice, Campden Instruments Ltd.) into flat hydrogel cylinders (thickness 2mm, diameter 9mm) and finally rehydrated and stored in PBS at 4°C. For 2D cellular *in vitro* studies, hydrogels of flat surfaces

Accepted Article

were prepared on top of coverslips for convenient handling (12 mm in diameter). The desired concentrations of DGL-G3 and PEG were mixed to prepare a final volume of 100 μ l and 60 μ l of the resulting solution were swiftly deposited between a hydrophobic glass slide and a round coverslip (for a hydrogel thickness of 0.6 mm). Hydrophobic glass slides were obtained by dipping in dichlorodimethylsilane (Sigma Aldrich) followed by overnight evaporation under a fume hood. After cross-linking, the hydrogel-covered coverslips were gently removed, sterilized overnight in EtOH:PBS (70:30, v/v) solution, washed 3x30 min with sterile PBS and kept at 4°C prior use. Concentrated hydrogels, which cross-linking time was faster than 10 s, were prepared in a cold room to slow down cross-linking.

2.2. Cross-linking speed

To monitor cross-linking speed, hydrogel components were added to a glass vial (8x25x35 mm) under agitation (300rpm) with a magnetic rod (5 mm) placed at exactly 4 cm from the magnetic stirrer. Cross-linking time was defined, in our study, as the time needed to halt the magnetic rod after adding all the hydrogel components. Three hydrogels per condition were used.

2.3. Swelling Ratio (Qs)

The swelling ratio (Qs) of 2 mm-thick dense hydrogels discs was determined in PBS at 37 °C. Prior incubation in PBS, samples were frozen in liquid nitrogen and freeze-dried to measure their dry weight. Samples were blotted before each weight measurement, performed at 1, 2, 6 and 24

Accepted Article

hours. The swelling ratio was defined as, $((W_s - W_i) / W_i)$, where W_s is the weight of swollen hydrogel and W_i is its initial dry weight after freeze-drying. Five hydrogels per condition were measured.

2.4. Mechanical testing

The mechanical properties of DGL/PEG hydrogels (2x9.1 mm) of different compositions were analyzed by cyclic compression with a dynamic mechanical analyzer (DMA 242 E Artemis, NEZSTCH). The hydrogel's domain of linearity was first determined with a strain sweep and compression test. Samples immersed in PBS were then subjected to compression at 10% strain and 60 μ m amplitude, with increasing frequencies (1-20 Hz) at room temperature. At least 5 hydrogels per condition were measured.

2.5. *In vitro* cell culture studies

Human dermal fibroblasts (Promocell, Heidelberg) were seeded at a density of 10,000 cell/cm² on the surface of hydrogel-covered coverslips and cultured in DMEM-F12 medium (Gibco) supplemented with 10% FBS (Life Technologies) and 1% penicillin/streptomycin (PAA Laboratories) at 37°C and 5% CO₂. Culture medium was refreshed every second day.

Hydrogels cytocompatibility was evaluated with a live/dead assay. Cells were washed once with

sterile PBS and incubated 30 min with a 6 μ M propidium iodide (Sigma Aldrich) and 1 μ M Calcein (Sigma Aldrich) solution and subsequently observed with a fluorescence microscope (Nikon TiE, Nikon Instruments). After observation, samples were washed with PBS, culture medium refreshed and cultured at 37°C and 5% CO₂ until next measurement. The number of alive and dead cells was determined from image analysis (Imagej⁽³²⁾), using 5 different fields of view randomly acquired per replicate of at least 7 hydrogels per condition. Viability was determined as the percentage of alive cells from the total number of cells. Cell adhesion was expressed as the total number of cells (alive or dead) present on the surface of the hydrogels 24 h post-seeding. The effect of hydrogel composition on cell morphology was evaluated by phase contrast microscopy (Nikon TiE) and by actin staining. Phase contrast microscopy pictures were acquired after 24h for 10 hydrogels per condition and at 72 h of culture for 5 hydrogels per condition. Cell spreading area, circularity and feret diameter of cells seeded were determined to compare cell morphologies. Control were only analyzed after 24 h, since cell confluence impeded images analysis after 72 h. F-actin cytoskeleton was observed by phalloidin (Sigma Aldrich) staining after 1, 3 and 8 days of culture. Cells on the hydrogels were fixed with 4% paraformaldehyde (PFA, Thermo Fischer Scientific) for 10 min followed by 20 min permeabilization with a 0.1% triton solution in PBS. After washing twice with PBS, the samples were incubated for 10 min with a 2 μ g/ml 4',6-Diamidino-2'-phenylindole

dihydrochloride (DAPI, Sigma Aldrich) and 2 $\mu\text{g/ml}$ phalloidin (Thermo Fischer Scientific) solution in PBS to stain the cell nucleus and actin cytoskeleton, respectively. Finally, hydrogels were observed with a fluorescence microscope (Nikon TiE). Cell proliferation was determined by counting DAPI stained cell nucleus after 1, 3 and 8 days of culture of 3 hydrogel per condition.

2.6. Preparation of porous hydrogels

Porous hydrogels were prepared by particulate/leaching technique using paraffin microspheres as porogens.⁽³³⁾ Briefly, 10 g paraffin (Histolab AB, Västra Frölunda) and 250 ml 0.5% poly(vinyl alcohol) (PVA, Sigma Aldrich) were heated to 80°C under stirring. After 20 min, the suspension was poured into ice water. The paraffin microspheres formed were sieved at 50, 100 and 180 μm and the resulting fractions were washed with distilled water, freeze-dried and conserved at 4°C.

To prepare porous hydrogels, 400 mg of paraffin microsphere, previously prepared, were compacted by centrifugation in 2ml microtubes (2000g, 10s) to obtain a flat surface.

Consecutively, DGL and PEG-NHS solutions were mixed by vortex and rapidly transferred to the microtubes containing the paraffin at 0°C. After cross-linking, the conical bottom of the microtubes was sectioned, paraffin was extracted with boiling EtOH for 40 min and the hydrogels were removed from the microtubes. Finally, hydrogels were cut into 2 mm thick discs with a vibratome. After that, the remaining paraffin was removed by several cycles (40 min) in reflux

EtOH. The obtained scaffold discs were sterilized overnight in EtOH 70%, washed 3x1h with sterile PBS, and kept at 4 °C prior use.

2.7. Biocompatibility

Biocompatibility of synthesized hydrogels was assessed by subcutaneous implantation of acellular hydrogels. After approval by local ethics committee, 5 hydrogels discs per condition (2x6 mm diameter) were implanted under the back skin of 8-weeks old SKH1 mice (Charles River, Ecully) under sedation by intraperitoneal xylazin-ketamin injection (four hydrogels per mouse). A small incision was performed at the low back of the mice and 4 subcutaneous pockets created with a sterile spatula. The hydrogels were inserted in the pockets and the incision sutured. Mice, fed ad libitum, were monitored every day for recovery and signs of distress. After three weeks, the mice were euthanized by anesthetic overdoses (intracardiac injection of sodium pentobarbital), the hydrogel samples recovered with surrounding tissue, fixed in 4% paraformaldehyde (PFA) solution in PBS, embedded in paraffin, sectioned and stained with Masson's trichrome. To highlight the penetration of blood vessels in the implanted hydrogels, sections of 3 different hydrogels per condition were stained for α -SMA (Abcam #ab5694 1:250) by immunohistochemistry, cell nuclei were counter-stained with 2 μ g/ml DAPI solution and observed by confocal microscopy (ZEISS, LSM 800). Round blood vessels with a diameter superior to 10 and 25 μ m per hydrogel cross section were counted by image analysis.

2.8. Statistical analysis

Statistical analyses were performed with Graphpad prism or Kaleidagraph. Test were performed using variance analysis (ANOVA). Data values are presented as mean \pm standard error (SE) and *p*-values of 0.05 and below were considered significant.

3. Results

3.1 Effect of reactants concentration on the formation of self-standing hydrogels

DGL/PEG hydrogel formation was straight forward. Concretely, hydrogels were obtained by covalent reaction between amine groups in the DGL and the NHS ester ends groups in PEG by simply mixing the solutions at room temperature (Figure 1.). Cross-linking velocity could be varied between 5 to 145 s by modifying reagent concentrations (between 1 to 4 mM for DGL and 19 to 30 mM for PEG-NHS), predominantly through the DGL concentration, as presented in Table 1. Interestingly, by considering the amount of amine groups and NHS functions theoretically available for the covalent reaction to occur, similar ratios of available amine to NHS functions resulted in different cross-linking velocities.

3.2 Swelling ratio

To mimic the physiological conditions, swelling ratio was determined in PBS at 37°C. As observed in Figure 2, the swelling was decreased with an increased concentration of DGL or PEG-NHS.

After 2 hours, a great quantity of liquid has been absorbed and reached equilibrium after 6 hours.

The composition with lowest concentration of both components showed the greatest swelling ratio of 22.89 ± 1.95 after 24 h.

3.3 Mechanical properties of dense DGL/PEG hydrogels

The mechanical properties of hydrogels of different compositions were measured with mechanical dynamical analysis. The loss (E''), storage (E') and complex modulus (E^*) were determined at increasing frequencies between 1 and 20 Hz. Figure 3 shows that for all hydrogels, E' was greater than E'' over the entire frequency range studied. This was further expressed by tan delta, which is the ratio of moduli (E''/E') that describes the viscous energy dissipation relative to the stored elastic energy. While E' was constant for all applied frequencies, E'' increased with frequency, which is a typical behavior of rubbery elastics⁽³⁴⁾. Overall, the complex modulus of the different hydrogels was increased with an increased concentration of PEG-NHS and DGL, varying from 7.7 ± 0.7 to 90.4 ± 28.8 kPa.

3.4 Cytocompatibility of the DGL/PEG hydrogels and effect of hydrogel composition on cell morphology and proliferation

Accepted Article

To assess the potential of the DGL/PEG hydrogels as a cell substrate, the adhesion and viability of human fibroblasts seeded on the flat surface of hydrogels of different compositions were evaluated with a live/dead assay (Figure 4.A). Seeded cells readily adhered on the hydrogels surface after 24 hours with a very low cytotoxicity, except for the hydrogel 3/19 mM (DGL/PEG), which showed a mortality of 79.4%. As shown in Figure 4.B, the hydrogel composition had an apparent effect on cell adhesion, concretely, with DGL concentration. With an increase of DGL, the total number of adhered cells was increased while adhesion was minimal when the DGL concentration was 1 mM. After 3 days of culture, compositions 1/19, 1/28 and 2/19 mM DGL/PEG presented around 84% of viability while more concentrated compositions (2/28 and 3/28 mM DGL/PEG) showed a viability of 97.9 and 96%, respectively (Figure 4.C), with no difference compared to controls (tissue culture plastic). Of note, an increase in PEG-NHS concentration resulted in an increase of the viability of the adhered cells.

Cell morphology was also modified by hydrogel composition (Figure 5.A). Cells on hydrogels with lower concentrations of DGL (1mM) and therefore lower percentage of adhesion presented a round morphology similar to non-adherent cells, with a mean circularity of 0.8 and a small ferret diameter (26.9–28.9 μm). An increase in hydrogel concentration had an impact on cell morphology. Except for hydrogel composition 2/28 and 3/28 (DGL/PEG) which showed a similar

cell morphology. After 72 hours, cell spreading area was increased in all compositions (Figure 5.B). The effect of hydrogel composition on cell morphology and spreading was further confirmed by phalloidin staining of f-actin fibres after 1, 3 and 8 days of culture (Figure 6.A.).

Regarding proliferation, seeded cells were able to proliferate over time (Figure 6.B), except for hydrogels with the lower concentration of DGL, where cells stayed round and showed proliferation rates close to zero. While hydrogels 2/28 and 3/28 mM showed similar proliferation rates of 69.9 ± 8.1 and 66.7 ± 14.6 , respectively, which were lower than tissue culture plastic controls (rate of 135.2 ± 26.19).

3.5 Biocompatibility

The behavior of DGL/PEG hydrogels of different compositions and porosities was evaluated *in vivo* by subcutaneous implantation in mice. As shown in Figure 7, regardless of pore size or composition, all hydrogels exhibited a mild foreign body reaction with the formation of a fibrous capsule after 3 weeks of implantation. All porous hydrogels were deeply infiltrated by cells, contrarily to dense hydrogels (Supplementary Figure 1). An important population of macrophages were visible, highly concentrated at the rim and within the porous implants and on the external edge of dense hydrogels. The macrophages were able to degrade the hydrogel through phagocytosis, further opening the pores, as exemplified in the blue close-ups on Figure 7.

Accepted Article

Interestingly, no granulocyte or lymphocytes could be observed, suggesting a mild inflammatory reaction. While the different porosities did not result in differences of cellular infiltration, the hydrogels composition clearly induced structural and degradation-related differences in the retrieved implants after 3 weeks. Softer hydrogels (7.7 ± 0.4 kPa) appeared condensed while harder ones (41.5 ± 5.0 and 76.7 ± 15.5 kPa) conserved their initial porous structure. Similar observations were made in regards of phagocytosis, with harder hydrogels being less prone to degradation by macrophages. The presence of neo-tissue within the hydrogels, revealing deposits of collagen, followed a similar pattern with an increased occurrence in harder hydrogels than in soft ones.

Curiously, an important amount of blood vessels were present within and throughout the porous hydrogels, as could be observed by IHC staining of α -SMA (Figure 8). Fewer blood vessels were present in soft hydrogels compared to more rigid compositions, with a preference to porous hydrogels with a broader range of pore size (50-180 μ m). When considering only the blood vessels with a diameter over 25 μ m, a preference to bigger pores was observed for more rigid compositions (Figure 8.B).

4. Discussion

PEG-based hydrogels have been the focus of much attention for various tissue engineering applications over the past years.⁽⁹⁾ However, their use with adherent cells requires them to be

functionalized or coated with other molecules and moieties to allow cells attachment and proliferation, which increase their complexity and decrease their practical applicability. With the aim of further broadening their potential by providing them with inherent cellular adhesion and interactions, we therefore defined and evaluated a novel hydrogel where homobifunctionalized PEG-NHS is cross-linked by poly(L-lysine) dendrigrafts (DGL). The straightforward mixing of PEG-NHS with DGL in aqueous solutions indeed results in the swift formation of self-standing hydrogels. Among the various dendrimer structures that have been associated with PEG to form hydrogels⁽²⁰⁾, DGL was so far never evaluated in this respect.

By varying the concentrations of hydrogel components, the cross-linking velocity, swelling and mechanical properties can be tailored. DGL of third generation used in this study presents an important density of amine groups on their surface (123), and it has been determined that only 97.7% of these amines residues are available as binding sites per molecules (114).⁽³⁵⁾ PEG-NHS, on the contrary, possess only two able NHS ester group per molecules. Hence, the ratio of available amines groups *versus* NHS is always higher than 1, but we did not observe a relationship between this ratio and the cross-linking speed, mechanical properties or swelling ratio. Indeed, solutions of increasing DGL and PEG-NHS concentrations but of similar amines/NHS ratios resulted in increasing cross-link velocities and mechanical properties. Similarly to PEG-PAMAM gels, the

Accepted Article

effect of the polymer content could be logically ascribed to an increase of cross-linking density due to a closer presence of the amine (DGL) and NHS (PEG) reactive groups. Once a PEG molecule is attached to the surface of the dendrimer, the second NHS function on the other end of the PEG chain will have lower mobility, which will increase its probability to react with an amine function on the same dendrimer and form intramolecular loops.⁽³⁶⁾ Therefore, the dilution of the reaction mixture increases the space between the dendrimers, forming many intramolecular loops at the expense of effective networks chains. Conversely, concentrating the mixture results in the opposite and increases the cross-link velocity.⁽³⁷⁾ This hypothesis is further reflected in the concomitant increase of mechanical properties and decrease of swelling observed in our hydrogels when increasing the polymer concentration. Since the arborescent molecules function as junction points in the cross-linking system, an increase in cross-links density will limit the expansion of the network, meaning a more compact mesh that leads to a decrease in swelling and an increase in rigidity. Similarly, Gitsov *et al.* observed that the swelling properties of hydrogels prepared from PEG and various dendritic fragments were not related to the PEG concentration or the dendrimer generation but mainly to the total increase in components concentration.⁽³⁸⁾

In addition to global polymer concentration, the DGL appears to have a predominant control of the hydrogel cross-linking. While its concentration doubling from 1 to 2 mM for a constant PEG-

NHS concentration induces a 10-fold increase of the cross-linking velocity, a 1.6-fold increase of PEG-NHS for a constant DGL concentration only marginally decreases cross-linking speed. Although a DGL presents 114 amine groups to act as a cross-linker, it is unlikely that all the end groups will be able to react with the PEG molecules due to steric crowding, which will limit the maximum number of PEGs that can be grafted to a single dendrimer.⁽³⁷⁾ The fact that an increase of PEG-NHS concentration for a constant DGL does not result in a significant increase of the cross-linking speed supports this hypothesis by indicating that a maximal number of PEG per DGL has been reached. Contrariwise, an increase of DGL at constant PEG-NHS allows to reduce the steric crowding and increases further the cross-linking velocity.

To provide to PEG hydrogels the ability to inherently interact with cells, our hypothesis that DGL bioactivity could be conveyed to the hydrogel bulk was confirmed, as human fibroblasts were able to adhere and proliferate on the surface of DGL/PEG hydrogels prepared without supplementary coating or functionalization before seeding. Similarly to DGLs coated on surfaces,⁽²⁹⁾ the ability of cells to attach and spread to DGL-containing hydrogels can be attributed to early electrostatic interactions between the polyanionic cell surfaces and the polycationic charges brought by the DGL's amino groups. This was further supported by the increase in cell adhesion with an increase in DGL concentration.

While the concentration of DGL plays a role in cell adhesion to the hydrogels, their viability seems dependent of the ratio between DGL and PEG-NHS. Mortality was indeed observed when the ratio of amines to NHS groups was greater than 9. The cationic nature of DGL that provides cell adhesion properties is possibly also the cause of their cytotoxic effect, since excessive cationic charges can affect the integrity of cell membranes.⁽³⁹⁾ When coupled with PEG molecules, PEG might shield the dendritic cationic charges and improve the DGL viability, similarly to Tang *et al.* who showed that PEG-gelation of DGL vectors for gene therapy allowed to decrease toxicity.⁽⁴⁰⁾ Unlike cell adhesion and viability, cell morphology and proliferation appear related to the overall hydrogel rigidity. For instance, for a constant DGL concentration (2mM), an increase of PEG-NHS concentration from 19 to 28 mM results in an increase of substrate rigidity (from 41.5 ± 5.0 to 90.4 ± 14.4 kPa) that is correlated with an increase of cell proliferation and a fusiform spread-like morphology. Similarly, an increase in DGL concentration for a given PEG (1/19 and 2/19 or 1/28 and 2/28 mM DGL/PEG) resulted in a more spread morphology and an increase in proliferation, only when the mechanical properties were also increased. Furthermore, without significant increase of substrate rigidity, fibroblasts showed similar morphology and proliferation rate, as could be observed for compositions 2/28 and 3/28 mM DGL/PEG. The importance of substrate rigidity, over hydrogel composition on cell morphology and proliferation was further

underlined in hydrogels of similar amine/NHS ratio but different overall polymer concentrations. For example, compositions 2/19 and 3/28 mM DGL/PEG have different rigidity (respectively, 41.5 ± 5.0 to 76.7 ± 15.5 kPa) and showed different cell proliferation and spreading. These observations are in good agreement with several groups that have showed an increase in cell spreading area, stress fibers and proliferation with an increase of substrate rigidity.^{(15),(41)–(45)} In our case, cell proliferation was indeed considerably lower on the DGL/PEG hydrogels as compared to the plastic controls. This is in good agreement with reported studies that showed a similar decrease of fibroblasts proliferation rate when seeded on collagen substrates^{(46),(47)}. In this regard, fibroblasts low proliferation rate on hydrogels can be considered closer to the physiological situation, where fibroblasts display a quiescent/secretory phenotype unless induced into proliferation by the release of stimulating factors as a result of tissue damage.⁽⁴⁸⁾

As could be expected from PEG-based materials,⁽⁴⁹⁾ no intense immune reaction was observed upon implantation of the DGL/PEG hydrogels under the back skin of mice for three weeks. Consequently, the presence of DGL does not seem to induce a specific inflammatory reaction. The controlled porosity in the hydrogels showed sufficient interconnection to allow cell ingrowth, vascularization and nutrient diffusion, which are important prerequisite for tissue engineering applications.^{(50)–(52)} Interestingly, broader pores size distribution in the hydrogels resulted in a

Accepted Article

higher vascularization, especially of vessels greater than 25 μm in diameter. Logically, bigger pores allow bigger blood vessels to penetrate the hydrogels; however, this could only be observed in rigid hydrogels since they are able to maintain their structure during implantation. In addition to a good biocompatibility and a good cellular infiltration, the important presence of blood vessels in the porous hydrogels is a further suggestion of the potential of these novel hydrogels to support tissue formation.

5. Conclusions

Through straight forward approaches, we have developed a novel PEG-hydrogel system cross-linked with DGL which inherently allows human dermal fibroblasts attachment and proliferation, without the need for any additional moieties. Macroscopically, the hydrogels cross-link velocity, swelling and rigidity can be tailored by the concentration of both components. As was hypothesized from the bioactive properties of DGLs, the ability of cells to adhere on the hydrogels surface appears solely dependent of the concentration of DGL while a minimal concentration of PEG is needed to sustain the viability of the adhered cells. Conversely, cell behavior and morphology appear linked to substrate rigidity rather than hydrogel composition. Of note, the resulting PEG-based hydrogels are biocompatible and allow cell infiltration and blood vessels invasion when porous. All these elements emphasize the potential of these novel hydrogels for a vast range soft tissue applications, while the presence of multiple amine groups and of a free

carboxylic acid function in the DGL opens the door to further modifications towards tailored features.⁽²⁷⁾

Acknowledgments

This work was supported by la Région Auvergne-Rhône-Alpes (grant 17 002601 ARC 2016), CONACyT, i²t² and the French national research grant DHERMIC (ANR TECSAN 016-01). The authors would like to thank the platform PriMaTiss for the histological sample preparation and the IGFL (UMR 5242) for the access to the vibratome.

Conflicts of Interest

The authors declare no conflict of interest.

References

1. Tibbitt MW, Anseth KS. Hydrogels as Extracellular Matrix Mimics for 3D Cell Culture. *Biotechnol Bioeng.* 2009;103:655–63.
2. Jia X, Kiick KL. Hybrid multicomponent hydrogels for tissue engineering. *Macromol Biosci.* 2009;9:140–56.
3. Park S, Park K. Engineered Polymeric Hydrogels for 3D Tissue Models. *Polymers (Basel).* 2016;8:23.
4. Figueiredo L, Pace R, D'Arros C, Réthoré G, Guicheux J, Le Visage C, Weiss P. Assessing glucose and oxygen diffusion in hydrogels for the rational design of 3D stem cell scaffolds in regenerative medicine. *J Tissue Eng Regen Med.* 2018;12:1238–46.
5. Van Vlierberghe S, Dubrue P, Schacht E. Biopolymer-based hydrogels as scaffolds for tissue engineering applications: a review. *Biomacromolecules* [Internet]. 2011;12:1387–408. Available from: <http://dx.doi.org/10.1021/bm200083n>
6. Franz S, Rammelt S, Scharnweber D, Simon JC. Biomaterials Immune responses to implants - A review of the implications for the design of immunomodulatory biomaterials. *Biomaterials* [Internet]. Elsevier Ltd; 2011;32:6692–709. Available from: <http://dx.doi.org/10.1016/j.biomaterials.2011.05.078>

- Accepted Article
7. Zhu J. Bioactive modification of poly(ethylene glycol) hydrogels for tissue engineering. *Biomaterials*. 2010;31:4639–56.
 8. Spicer CD. Hydrogel scaffolds for tissue engineering: the importance of polymer choice. *Polym Chem. Royal Society of Chemistry*; 2020;11:184–219.
 9. Lin C, Anseth KS. PEG Hydrogels for the Controlled Release of Biomolecules in Regenerative Medicine. *Pharm Res*. 2009;26:631–43.
 10. Sargeant TD, Desai AP, Banerjee S, Agawu A, Stopek JB. An in situ forming collagen – PEG hydrogel for tissue regeneration. *Acta Biomater* [Internet]. *Acta Materialia Inc.*; 2012;8:124–32. Available from: <http://dx.doi.org/10.1016/j.actbio.2011.07.028>
 11. Barros D, Conde-sousa E, Gonçalves AM, Han WM, García AJ, Amaral IF, Pêgo AP. Engineering hydrogels with affinity-bound laminin as 3D neural stem cell culture systems. *Biomater Sci. Royal Society of Chemistry*; 2019;7:5338–49.
 12. Hern DL, Hubbell JA. Incorporation of adhesion peptides into nonadhesive hydrogels useful for tissue resurfacing. *J Biomed Mater Res*. 1998.
 13. Ouyang L, Dan Y, Shao Z, Yang S, Yang C, Liu G, Duan D. MMP - sensitive PEG hydrogel modified with RGD promotes bFGF , VEGF and EPC - mediated angiogenesis. *Exp Ther Med*. 2019;18:2933 –41.
 14. Burdick JA, Anseth KS. Photoencapsulation of osteoblasts in injectable RGD-modified PEG hydrogels for bone tissue engineering. 2002;23:4315–23.
 15. Nemir S, L. West J. Synthetic Materials in the Study of Cell Response to Substrate Rigidity. *Ann Biomed Eng*. 2010;38:2–20.
 16. Papavasiliou G, Sokic S, Turturro M. Synthetic PEG Hydrogels as Extracellular Matrix Mimics for Tissue Engineering Applications. *Biotechnol - Mol Stud Nov Appl Improv Qual Hum Life*. 2012.
 17. Rizzi SC, Hubbell JA. Recombinant Protein-co-PEG Networks as Cell-Adhesive and Proteolytically Degradable Hydrogel Matrixes. Part I: Development and Physicochemical Characteristics. *Biomacromolecules*. 2005;6:1226–38.
 18. Wathier M, Jung PJ, Carnahan MA, Kim T, Grinstaff MW. Dendritic Macromers as in Situ Polymerizing Biomaterials for Securing Cataract Incisions. *J Am Chem Soc*. 2004;126:12744–5.
 19. Wathier M, Johnson CS, Kim T, Grinstaff MW. Hydrogels Formed by Multiple Peptide Ligation Reactions To Fasten Corneal Transplants. *Bioconjugate Chem*. 2006;17:873–6.
 20. Kaga S, Arslan M, Sanyal R, Sanyal A. Dendrimers and Dendrons as Versatile Building Blocks for the Fabrication of Functional Hydrogels. *Molecules*. 2016;21.
 21. Oliveira JM, Salgado AJ, Sousa N, Mano JF, Reis RL. Dendrimers and derivatives as a potential therapeutic tool in regenerative medicine strategies—A review. *Prog Polym Sci* [Internet]. Elsevier Ltd; 2010;35:1163–94. Available from: <http://linkinghub.elsevier.com/retrieve/pii/S0079670010000456>

- Accepted Article
22. N. Desai P, Yuan Q, Yang H. Synthesis and Characterization of Photocurable Polyamidoamine Dendrimer Hydrogels as a Versatile Platform for Tissue Engineering and Drug Delivery. *Biomacromolecules*. 2011;11:666–73.
 23. Navath RS, Menjoge AR, Dai H, Romero R, Kannan S, Kannan RM. Injectable PAMAM Dendrimer À PEG Hydrogels for the Treatment of Genital Infections : Formulation and in Vitro and in Vivo Evaluation. *Mol Pharm*. 2011;8:1209–23.
 24. Unal B, Hedden RC. Gelation and swelling behavior of end-linked hydrogels prepared from linear poly (ethylene glycol) and poly (amidoamine) dendrimers. *Polymer (Guildf)*. 2006;47:8173–82.
 25. Labieniec-Watala M, Watala C. PAMAM dendrimers: Destined for success or doomed to fail? Plain and modified PAMAM dendrimers in the context of biomedical applications. *J Pharm Sci [Internet]*. Elsevier Masson SAS; 2015;104:2–14. Available from: <http://dx.doi.org/10.1002/jps.24222>
 26. Romestand B, Rolland J, Commeyras A, Desvignes I, Pascal R, Vandenamee-trambouze O. Dendrigrift Poly- L -lysine : A Non-Immunogenic Synthetic Carrier for Antibody Production. *Biomacromolecules*. 2010;11:1169–73.
 27. Francoia J, Vial L. Everything You Always Wanted to Know about Poly-l-lysine Dendrigrifts (But Were Afraid to Ask). *Chem A Eur J*. 2018;24:1–10.
 28. Huang R, Liu S, Shao K, Han L, Ke W, Liu Y, Li J, Huang S, Jiang C. Evaluation and mechanism studies of PEGylated dendrigrift poly-L-lysines as novel gene delivery vectors. *Nanotechnology [Internet]*. 2010;21:265101. Available from: <http://www.ncbi.nlm.nih.gov/pubmed/20522929>
 29. Lorion C, Faye C, Maret B, Trimaille T, Régnier T, Sommer P, Debret R. Biosynthetic support based on dendritic poly(L-lysine) improves human skin fibroblasts attachment. *J Biomater Sci Polym Ed [Internet]*. 2014 [cited 2016 Feb 3];25:136–49. Available from: <http://www.ncbi.nlm.nih.gov/pubmed/24116875>
 30. Collet H, Souaid E, Cottet H, Deratani A, Boiteau L, Dessalces G, Rossi JC, Commeyras A, Pascal R. An expeditious multigram-scale synthesis of lysine dendrigrift (DGL) polymers by aqueous n-carboxyanhydride polycondensation. *Chem - A Eur J*. 2010;16:2309–16.
 31. Maret B, Crépet A, Faye C, Garrelly L, Ladavière C. Molar-mass analysis of dendrigrift poly(L-lysine) (DGL) polyelectrolytes by SEC-MALLS: The “cornerstone” refractive index increment. *Macromol Chem Phys*. 2015;216:95–105.
 32. Schneider CA, Rasband WS, Eliceiri KW. NIH Image to ImageJ: 25 years of image analysis. *Nat Methods [Internet]*. Nature Publishing Group; 2012 [cited 2019 Oct 25];9:671–5. Available from: <http://www.nature.com/articles/nmeth.2089>
 33. Ma PX, Choi PDJ. Biodegradable Polymer Scaffolds with Well-Defined Interconnected Spherical Pore Network. *Tissue e Eng*. 2001;7:23–33.
 34. Anseth KS, Bowman CN, Brannon-Peppas L. Mechanical properties of hydrogels and their experimental

- determination. *Biomaterials*. 1996;17:1647–57.
35. Coussot G, Nicol E, Commeryras A, Desvignes I, Pascal R, Vandenabeele-trambouze O. Colorimetric quantification of amino groups in linear and dendritic structures. *Polym Int*. 2009;58:511–8.
36. Wang Y, Zhao Q, Zhang H, Yang S, Jia X. A novel poly(amido amine)-dendrimer-based hydrogel as a mimic for the extracellular matrix. *Adv Mater*. 2014;26:4163–7.
37. Unal B, Hedden RC. Gelation and swelling behavior of end-linked hydrogels prepared from linear poly (ethylene glycol) and poly (amidoamine) dendrimers. *Polym J*. 2006;47:8173–82.
38. Gitsov I, Zhu C. Amphiphilic hydrogels constructed by poly(ethylene glycol) and shape-persistent dendritic fragments. *Macromolecules*. 2002;35:8418–27.
39. Quinton MP, Philpott CW. A Role for Anionic Sites in Epithelial Architecture: Effects of Cationic Polymers on Cell Membrane Structure. *J Cell Biol*. 1978;56:787–96.
40. Tang M, Dong H, Li Y, Ren T. Harnessing the PEG-cleavable strategy to balance cytotoxicity, intracellular release and the therapeutic effect of dendrigraft poly-L-lysine for cancer gene therapy. 1284 | *J Mater Chem B* [Internet]. 2016 [cited 2019 Oct 21];4:1284. Available from: www.rsc.org/MaterialsB
41. Jiang G, Huang AH, Cai Y, Tanase M, Sheetz MP. Rigidity Sensing at the Leading Edge through avb3 Integrins and RPTPa. *Biophys J*. 2006;90:1804–9.
42. Yeung T, Georges PC, Flanagan LA, Marg B, Ortiz M, Funaki M, Zahir N, Ming W, Weaver V, Janmey PA. Effects of Substrate Stiffness on Cell Morphology , Cytoskeletal Structure , and Adhesion. *Cell Motil Cytoskeleton*. 2005;60:24–34.
43. Ghosh K, Pan Z, Guan E, Ge S, Liu Y, Nakamura T, Ren XD, Rafailovich M, Clark RAF. Cell adaptation to a physiologically relevant ECM mimic with different viscoelastic properties. *Biomaterials*. 2007.
44. Lo CM, Wang HB, Dembo M, Wang YL. Cell movement is guided by the rigidity of the substrate. *Biophys J* [Internet]. Elsevier; 2000;79:144–52. Available from: [http://dx.doi.org/10.1016/S0006-3495\(00\)76279-5](http://dx.doi.org/10.1016/S0006-3495(00)76279-5)
45. Solon J, Levental I, Sengupta K, Georges PC, Janmey PA. Fibroblast Adaptation and Stiffness Matching to Soft Elastic Substrates. *Biophys J*. 2007;93:4453–61.
46. Kono T, Tanii T, Furukawa M, Mizuno N, Kitajima J, Ishii M, Hamada T, Yoshizato K. Cell cycle analysis of human dermal fibroblasts cultured on or in hydrated type I collagen lattices. *Arch Dermatol Res*. 1990;282:258–62.
47. Rhudy RW, McPherson JM. Influence of the extracellular matrix on the proliferative response of human skin fibroblasts to serum and purified platelet-derived growth factor. *JCell Physiol*. 1988;137:185 –91.
48. Sarber R, Hull B, Merrill C, Sorzano T, Bell E. Regulation of proliferation of fibroblasts of low and high population doubling levels grown in collagen lattices. *Mech Ageing Dev*. 1981;17:107–17.
49. Lynn AD, Kyriakides TR, Bryant SJ. Characterization of the in vitro macrophage response and in vivo host response to poly(ethylene glycol)-based hydrogels. *J Biomed Mater Res - Part A*. 2010;93:941–53.

50. J. Griffon D, Sedighi MR, Schaeffer D V., Eurell JA, Jonhson AL. Chitosan scaffolds : Interconnective pore size and cartilage engineering. *Acta Biomater.* 2006;2:313–20.
51. Rouwkema J, Rivron NC, Blitterswijk CA Van. Vascularization in tissue engineering. *Trends Biotechnol.* 2008;26:434–41.
52. Annabi N, Nichol JW, Zhong X, Ji C, Koshy S, Khademhosseini A, Dehghani F. Controlling the porosity and microarchitecture of hydrogels for tissue engineering. *Tissue Eng Part B Rev [Internet].* 2010 [cited 2015 Dec 5];16:371–83. Available from: <http://www.pubmedcentral.nih.gov/articlerender.fcgi?artid=2946907&tool=pmcentrez&rendertype=abstract>

Figures

Figure 1. Photographs of the hydrogel at room temperature A) Dense 2/19 mM DGL/PEG hydrogel disc of 2mm thickness and 9.1mm diameter. B) Hydrogel in an inverted conic tube.

*Figure 2. Swelling ratio of hydrogels of different compositions (hydrogel concentration is expressed as the ratio DGL/PEG in mM) swelling measured in PBS at 37°C. (n= 5, Two-way ANOVA, $p < 0.05$ * at 24 hours).*

*Figure 3. Mechanical properties of dense hydrogel discs (2x9.1mm) of different compositions (hydrogel concentration is expressed as de ratio DGL/PEG in mM) measured at room temperature under PBS immersion by dynamical mechanical analysis in compression at a 10% strain and 60 μ m of amplitude. A) complex modulus, B) tan delta, C) storage modulus and D) loss modulus. (n=7, Two-way ANOVA, $p < 0.05$, *compared to 1/19, τ compared to 1/28 and γ compared to 2/19).*

*Figure 4. Dermal human fibroblast viability. A) Cytotoxicity by live/dead assay after 1 and 3 days of culture on the surface of hydrogels of different compositions (hydrogel concentration is expressed as de ratio DGL/PEG in mM). Live cells are observed in green and dead cells in red B) Total cell adhesion after 24 hours of cell seeding on top of hydrogels of different compositions. (n=7, One-way ANOVA, $p < 0.05$, *compared to*

control, τ compared to 1/19 and γ compared to 1/28) C) Viability percentage obtained from images analysis ($n=7$, $p < 0.05$ * compared to control).

Figure 5. Dermal fibroblast morphology when cultivated on the surface of hydrogels of different compositions (hydrogel concentration is expressed as de ratio DGL/PEG in mM) A) contrast phase photos after 24 hours and 72 hours of cell seeding B) Morphology parameters (spreading area, circularity and feret diameter) obtained from image analysis of contrast phase photos of ten hydrogels at 24h and five hydrogels after 72h. Control was only analyzed after 24 hours since after 72 hours images analysis was not possible due to cell confluence. ($p < 0.05$, * compared to control at 24 hours).

Figure 6. A) Cytoskeleton structure of dermal fibroblasts seeded on the surface of hydrogel of different compositions (hydrogel concentration is expressed as de ratio DGL/PEG in mM) observed by DAPI-Phalloidin staining after 1, 4 and 8 days of culture (in blue cell nuclei and in red actin fibers). B) Cell proliferation rate of fibroblasts seeded on the surface of hydrogel of different compositions (hydrogel concentration is expressed as de ratio DGL/PEG in mM) obtained from cell nuclei counting after 1, 4 and 8 days of culture. ($n=3$, One-way ANOVA, $p < 0.05$, *compared to control, τ compared to 1/19 and γ compared to 1/28).

Figure 7. Subcutaneous implantation in mice for three weeks of DGL/PEG porous hydrogels of different compositions (soft, medium and rigid, 7.7 ± 0.4 , 41.5 ± 5.0 and 76.7 ± 15.5 kPa, respectively) and with different pore sizes distribution. Masson's trichrome staining of the full explants and close-ups highlighting the hydrogel (#), the fibrous capsule (*), macrophages (+), synthesised collagen (α) and blood vessels (Φ).

Figure 8. Blood vessels present after three weeks of subcutaneous implantation in mice in porous hydrogels of different compositions (soft, medium and rigid, 7.7 ± 0.4 , 41.5 ± 5.0 and 76.7 ± 15.5 kPa, respectively) A) Immunofluorescence staining of α -SMA (red) indicating blood vessels present within the porous hydrogels while cell nuclei are stained with

DAPI in blue; white lines delimit the border of the hydrogel and arrows point to sectioned blood vessels. B) Number of blood vessels present in the hydrogel of a diameter greater than 10 μ m or 25 μ m obtained from image analysis of mosaic images of complete slides of porous hydrogels. (n=3, Two-way ANOVA, * p<0.05).

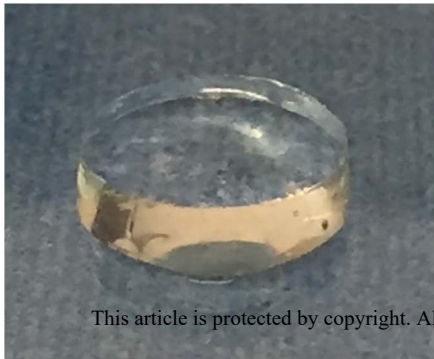
Tables

Table 1. Cross-linking time to form self-standing hydrogels in relation to the final concentration of DGL and PEG-NHS and ratio of available amine/NHS functions (Two-way ANOVA between PEG and DGL concentration, * indicates that there is a statistically significant difference when DGL concentration is modified, for any given PEG concentration, p<0.05, n=3)

Supplementary data

Supplementary figure 1. Subcutaneous implantation of dense DGL/PEG hydrogel (2/19mM DGL/PEG). Masson's trichrome staining of the full explants and close-ups highlighting the hydrogel (#), the fibrous capsule (*), macrophages (+).

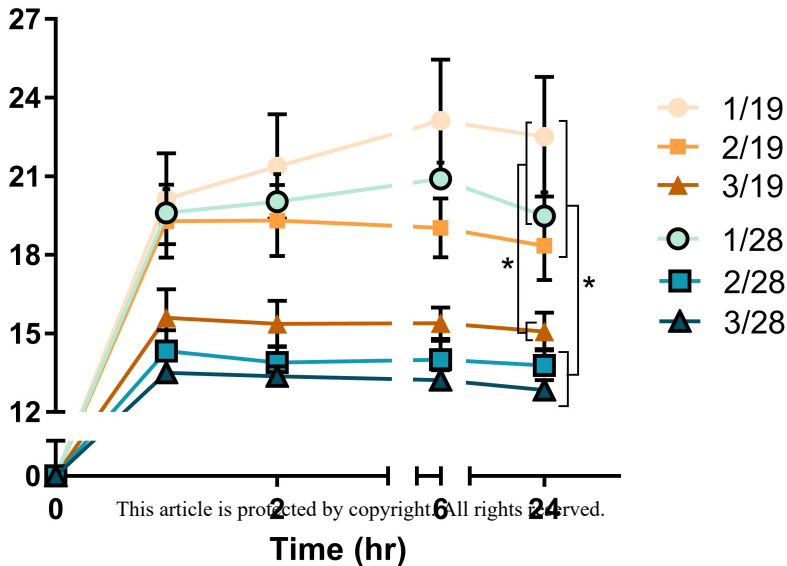
A)



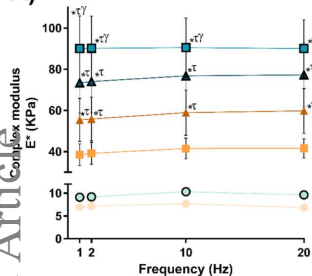
B)



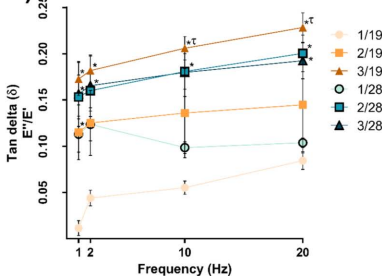
This article is protected by copyright. All rights reserved.



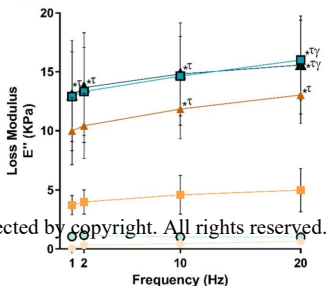
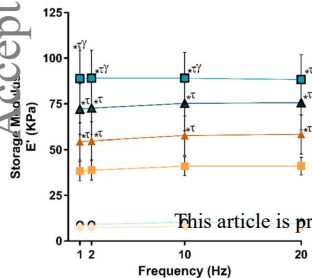
A)



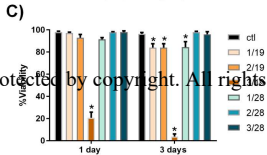
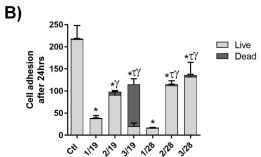
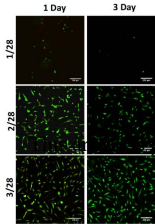
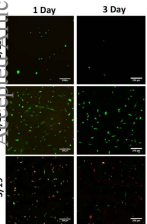
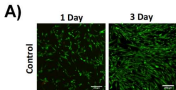
B)

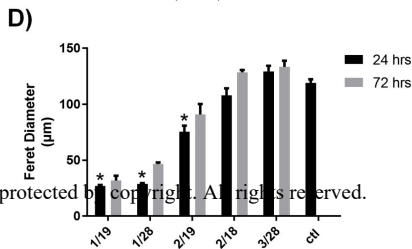
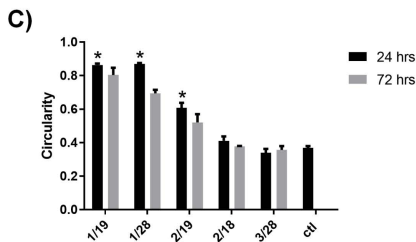
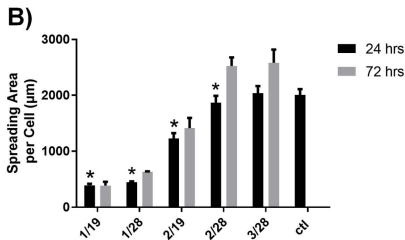
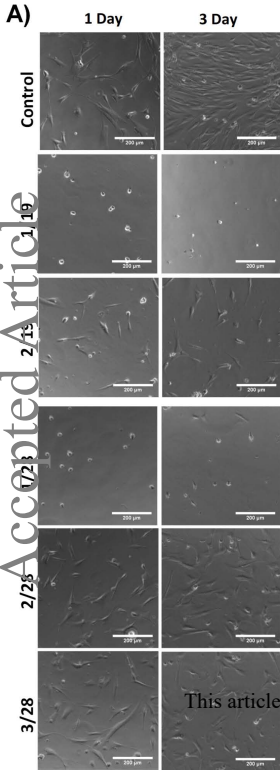


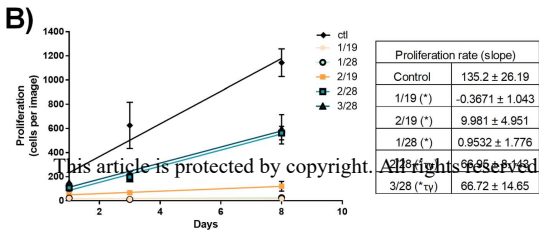
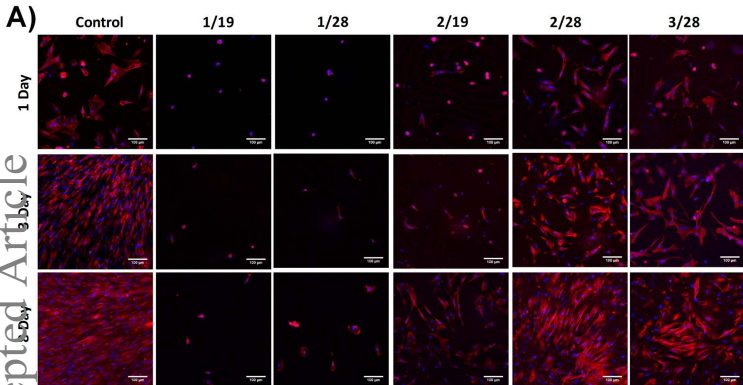
D)



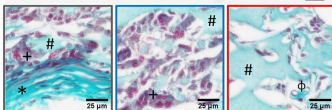
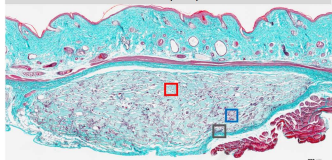
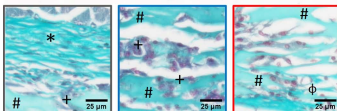
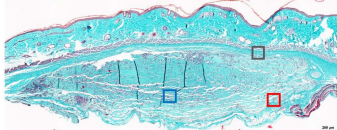
This article is protected by copyright. All rights reserved.



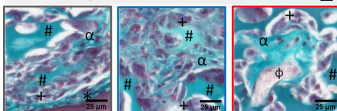
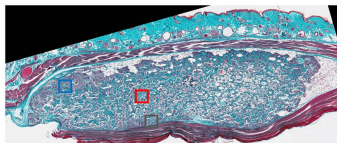
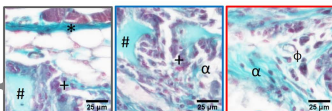
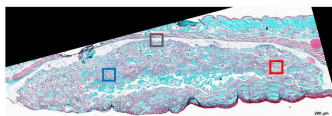




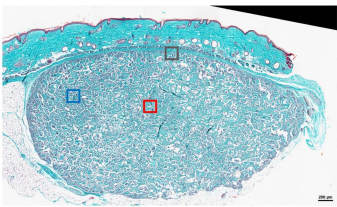
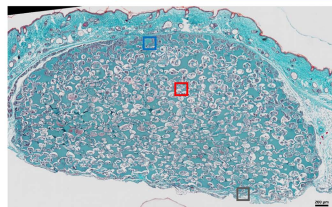
Soft

100 % of 100-180 μm paraffin beads25 % of 100-180 μm paraffin beads and 75 % of 50-100 μm paraffin beads

Medium



Rigid



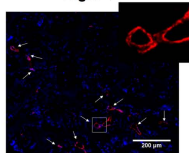
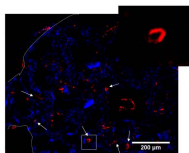
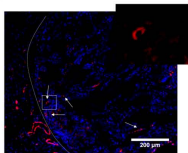
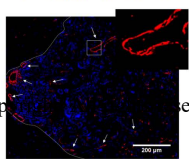
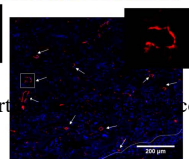
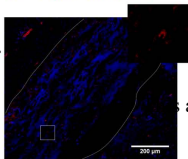
This article is protected by copyright. All rights reserved. φ

A)

Soft

Medium

Rigid

50-100 μm 75% 50-100 μm
25% 100-180 μm 

B)

■ Soft ■ Medium ■ Rigid

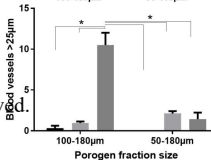
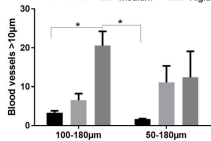


Table 1. Crosslinking time to form self-standing gels in relation to the final concentration of DGL and PEG-NHS and ratio of available amine/NHS functions (Two-way ANOVA between PEG and DGL concentration, * indicates that there is a statistically significant difference when DGL concentration is modified, for any given PEG concentration, $p < 0.05$, $n=3$)

Time (s) (Ratio amines/NHS)		PEG-NHS (mM) (Available NHS, mM)		
		19 (38)	28 (56)	30 (60)
DGL (mM) * (Available amines, mM)	1 (114)	144.6 ± 23.3 (3)	122.0 ± 24.0 (2.03)	140.2 ± 15.8 (1.9)
	2 (228)	14.94 ± 1.1 (6)	13.17 ± 1.9 (4.07)	12.28 ± 3.5 (3.8)
	3 (342)	10.47 ± 4.5 (9)	8.4 ± 1.2 (6.1)	7.66 ± 1.1 (5.7)
	4 (456)	6.77 ± 0.9 (12)	4.76 ± 0.6 (8.14)	5.47 ± 0.6 (7.6)